8-2-2023 10:00 AM

# The Modulation of LFP Characteristics In The Freely Moving Common Marmoset

William JM Assis, *Western University*

Supervisor: Martinez-Trujillo, Julio C., *The University of Western Ontario*

A thesis submitted in partial fulfillment of the requirements for the Master of Science degree in Neuroscience

# Abstract

The hippocampus is a neural structure critical for navigation. Neurons in this region, along with others, create a functional network which generates large-amplitude modulations known as local field potential (LFP) activity. Prior LFP research has predominantly used rodent animal models, however recent studies have shown that frequencies associated with navigation in other mammals do not correlate to those of the rodent. We hypothesized that LFP characteristics in the common marmoset are modulated by the speed and axis of travel of the animal. Two marmosets were placed in a free moving 3-dimensional environment where movement and neurological activity were recorded. Results showed LFP modulation based on movement, including significant changes in power with movement speed and vertical motion. We provide evidence of theta bout activity and other non-rodent-like characteristics, prompting discussion on the generalization of findings in rodent models such as mice and rats to primate navigation.



Keywords

Electrophysiology, Local Field Potential, Hippocampus, Common Marmoset, NHP, Theta, Beta, Navigation.

# Summary for Lay Audience

The region of the brain in mammals responsible for navigation is found in the medial temporal lobe, known as the hippocampus. Neurons in the hippocampus produce brain waves called local field potentials (LFP). These LFPs can be broken down into the different frequency oscillations and their relative contribution (power), allowing the analysis of specific frequency bands. These LFPs are thought to be linked to neural function as they are a product of populations of neurons synchronously firing and are predominantly correlated to certain behaviors. The vast majority of prior LFP research has been conducted using rodent animal models such as rats and mice, but recent studies have shown that LFPs associated with navigation in other mammals (bats, monkeys, humans) do not show the same features as the rodent's LFPs. Here, we looked to analyze the modulation of LFP profiles in the common marmoset in a freely moving 3-dimensional environment. The animals had the ability to freely move in a plexiglass enclosure while their movement and neural activity recorded was in real time. Taking this data, we divided movement into five categories: stationary, horizontal-slow, horizontal-fast, vertical-up, and vertical-down. We hypothesized that the marmoset's speed and direction of motion influence features of hippocampal LFPs. Our results show that LFP profiles change based on movement speed and direction of travel, stationary and vertical movement being on opposite ends of the spectrum in regard to LFP frequency power. We also provide evidence that marmosets have similar LFP profiles as other primates in the theta frequency band associated with navigation, which is not modulated by the speed of movement while in motion. These findings provide further evidence of non-rodent-like characteristics exhibited in marmosets, prompting discussion on the generalization of findings in rodent models, such as mice and rats, to primate navigation.

# Co-Authorship Statement

| **Contribution to this thesis** | |
|---|---|
| Animal husbandry, training, and care | WA, DB, KT, KG |
| Surgical implantations | WA, JM, DB, JS, BC, KT, KG |
| Common marmoset neural and movement data sets | DB |
| MATLAB Script for analysis of recordings | WA, JD, DB, LP |
| Data analysis and interpretation | WA |
| Revision of manuscript | JM, BC |
| Supervision of the project | JM |

| | |
|---|---|
| William Assis (Candidate) | Julio Martinez-Trujillo (PI) |
| Brian Corneil (Thesis Reader) | Jarrod Dowdall |
| Diego Buitrago-Piza | Laxan Premachandran |
| Ben Corrigan | Julia Sunstrum |
| Kim Thomaes | Kristy Gibbs |

# Acknowledgments

I first wish to acknowledge and thank my supervisor, Dr. Julio Martinez-Trujillo, for his guidance and support during my tenure in his lab. Julio gave me an opportunity in life that I will always be grateful for and will never forget. I am thankful for all he has done for me over the years, and most recently his unflinching support in my decision to alter my career path.

Thank you to all those who acted in my advisory committee: Drs Brian Corneil, Wataru Inoue, Stefan Everling, and Stephen Lomber.

Thank you to Jarrod Dowdall, this thesis would not have been possible without your expertise in the field and willingness to mentor me in LFP science as much as you did.

I want to thank the fantastic administrators of the Western Neuroscience department: Dr Brian Corneil (Department Director), Susan Simpson (Program Coordinator), and Lara Staecker (Administrative Assistant). Your guidance and patience in helping me navigate the challenges posed by my military service was above and beyond what I could have ever asked for.

To my fellow trainees on "the 7th", thank you. You were the wind in my sails and helped more than you realize.

# Dedication

To Maria, for everything.

# Table of Contents

# List of Tables

# List of Figures

# List of Appendices

# Chapter 1

## 1 Introduction

The hippocampus (HPC) is a phylogenetically ancient structure within the mammalian brain. The HPC formation is found within the medial temporal lobe, comprised of multiple regions including the Cornu Ammonis (CA), Entorhinal Cortex (EC), Dentate Gyrus (DG) and Subiculum (SB)[1]. The HPC operates in a complex pathway which enables high-order cortical regions to converge to a single network in the CA3. This is achieved through inputs entering the HPC via the perforant path from the EC, synapsing with the DG then projecting to CA3. CA3 projects via the Shaffer collaterals to CA1, which connects to the SB, then the neocortex. One theory of how this complex network operates proposes that the hippocampal CA3 system operates as a single attractor or auto association network[2]. This sees the DG perform pattern separation, which through its projections to CA3, provides a mechanism for recall cues in the CA3. CA1 then recodes information from CA3 to establish associatively learned back projections to the neocortex (Figure 1). This process then enables the recall of information back to the neocortex as necessary, aka remembering[3,4]. The method by which the HPC sends signals across its various structures are known as ‘spikes’. This term refers to how neurons encode information by varying the rate and timing of action potential firing[5]. Through the analysis of spike firing variation, we can define when a structure is preferentially, or selectively, firing. This type of firing occurs when specific tissues exhibit an increase in activity, or ‘burst’, when a set of conditions in the animal’s environment or its sensory reception are met. Within the HPC, preferential firing can be observed during navigation.

The HPC has become widely known for its active role in navigation and associative memory, in both the real and virtual world [6,7]. This is thanks to navigation cells. In 1976 John O’Keefe published on the discovery of HPC cells in the rat that preferentially fired depending on the animal’s location in its environment, which he aptly named “place cells”[8]. Since then, additional cells that act as navigational enablers have been characterized, such as grid cells which fire at regular intervals as the animal traverses an

open environment, and border cells, which fire in response to a boundary at a specific distance and direction to the animal[9,10].

As individual neurons are incapable of complex operations alone, it is the functional networks of synchronized activity which generate large-amplitude modulations of local field potentials (LFPs)[11]. Neuronal synaptic activity from the dendrites and somata are often the most important source of extracellular current flow[12], with currents overlapping in time to induce a measurable signal, thus enabling LFP recordings[13]. Within the HPC, these signals are mainly attributed to pyramidal cells, the primary excitatory neurons of the HPC. There are also the HPC interneurons which synchronize activity across large neuronal groups due to their divergent projections[14]. Notably, within CA1 pyramidal neurons and interneurons are densely packed and aligned in parallel. This results in a summated current flow and large amplitude signals which are easily detected by LFP recordings[15].

In the rat model, place cell spiking has been correlated to theta (4-10 Hz) rhythmicity. A phenomenon known as ‘theta phase precession’ occurs when spikes fire at successively earlier phases of the theta rhythm (Figure 2). This correlates best with distance travelled through the place field, and provides a phase code in addition to rate of fire coding[16]. This relationship between theta oscillations and place cell function is well established in the rat model and is further discussed in Chapter 1.2.

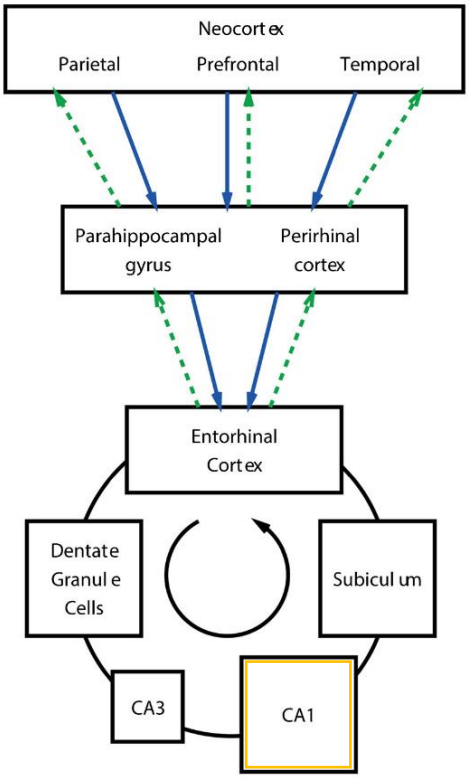


**Figure 1.** Block diagram of pathways within the hippocampal formation.

The hippocampus receives inputs from the neocortex via the perforant pathway to the entorhinal cortex for processing via the DG, CA 3, and CA 1. This then feeds into the subiculum, enabling back projections to the neocortex[3]. Array recordings used in this thesis are recorded from the CA 1 region of the Common Marmoset (see Figure 4 & Table 1).

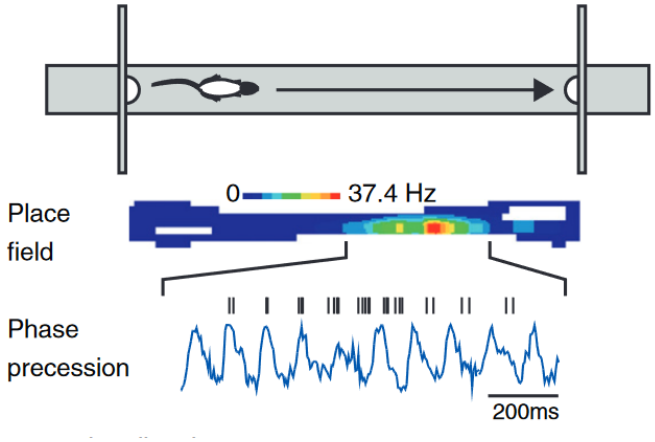


**Figure 2.** Theta-phase precession of place cell firing in rats.

Illustration depicting place cell activity as an animal runs down a track[16]. The spike rate of fire correlates to theta oscillations, where spikes (depicted as ticks), fire at successively earlier phases of theta rhythm. This results in the theta phase of firing correlating with the distance travelled through the field.

## 1.1 Frequency Bands

There are several brain rhythms observed in the non-human primate (NHP) hippocampus, namely delta δ (< 4Hz), theta θ (4-8Hz), alpha α (8-13Hz), beta β (14-30Hz) and gamma γ bands (> 30Hz)[17]. These oscillation frequencies are observed during specific behavioral conditions and are generated by different neural regions; thus the common hypothesis is that they enable specific functions. Human brain oscillations were first discussed by German psychiatrist Hans Berger, and published in 1929[18]. He classified neural oscillations as alpha waves, which were disrupted by the subject opening their eyes when in a lying relaxed state, or exerting mental effort[17]. Since then, many studies have associated alpha oscillations with processes originating from the occipital cortex and visual thalamus[19,20], and are believed to play a role in the suppression of irrelevant/unattended information[21].

Beta oscillations have been observed in the sensorimotor (parietal) cortex in relation to motor function, with increased activity during movement preparation[22], tactile forelimb exploration[23], and isometric contractions[24]. Beta frequency activity has been observed

synchronized between muscle and motor cortical areas[25,26], as well as between different components of the sensorimotor cortex[27,28]. Moreover, it has been demonstrated that beta oscillations act as a mechanism for binding distributed somatosensory and motor cortical areas into a functional network[29], providing information to the sensorimotor system to control motor output[30]. This has recently been observed with beta oscillations acting as a 'stop' command during stationary 'microfalls', enacting motor control for recovery[31]. Beta rhythms have also been suggested to play a key role in "top-down" tasks between the frontal and parietal cortices[32], where voluntary attention shifts may use beta synchrony to help resolve competition for attentional selection[33,34]

The final frequency investigated in this thesis is the theta rhythm. This band was discovered in 1938, and its association to memory established in 1972. This association was established through the observed correlation between the proportion of theta oscillations recorded, and the degree at which rats remembered experienced foot shocks[35]. These rhythms were widely believed to originate from the Medial Septum's (MS) GABAergic pacemaker interneurons[36], which provide phase-locked theta rhythms to the HPC[37]. However, this foundation has been challenged by the discovery of theta frequency spontaneity of *in vitro* HPC cells, with results suggesting theta rhythm genesis from local interactions between HPC interneurons and pyramidal cells[38]. As previously discussed, these oscillations play a critical role in HPC navigation cells, notably place and grid cells. These HPC cells provide positional information for the animal as it navigates, demonstrating selective firing depending on its location and thus sequence of events of its trajectory[39].

## 1.2 Animal Models

Theta oscillations have been demonstrated as critical in rodent navigation synchronizing place cell function, with performance impaired by the disruption of theta rhythms[40]. In the rodent model, these oscillations are continuous and act as a travelling wave which begins when the rat starts navigating, and ends for foraging or grooming[41]. In contrast, electrophysiological studies in fruit bats have observed the opposite; navigational cell activity with little to no theta activity[42]. In these bat models, theta oscillations were recorded in short bouts (rather than continuous), and a lack of place cell modulation

during flight [43], and grid cells while crawling[42]. With these observations, studies have suggested different grid-cell coding mechanisms between rats and bats due to the lack of theta resonance in the bat[44]. This difference in theta continuity has also been observed in NHP[45] and human studies[46], where theta rhythms are only observed in short theta bouts rather than continuously. This contrast has been hypothesized to be attributed to the activity of the animal, where rodent studies are comprised of foraging tasks which are natural behaviours with a combination of sensory cues (visual, tactile, olfactory), vs primate and human studies which have primarily been artificial activities (including virtual) with the sole sensory input being visual[47]. This theory though is inconsistent with the observed lack of theta rhythms in bats during flight (which is their natural movement) leading to the question of whether theta rhythms act in bouts or continuously due to differences between species, or the experimental task the model was subjected to.

One animal model which has recently become popular is the common marmoset (*Callithrix jacchus*). This new-world primate has received increased interest and use as a research model in neuroscience. This increase in popularity was primarily as a result of its potential as a transgenic model[48,49], as well as its smooth (lissencephalic) cortex, small size, low cost, ease of handling, and high fecundity[50]. Due to these advantages, the marmoset has become known as a model in between the highly studied but evolutionary-distant rodent, and the closer related rhesus macaque, a model that has been extensively used to investigate neural substrates of human behavior and cognitive function[51].

To our knowledge there are currently only two peer-reviewed publications which investigate theta rhythms in the common marmoset. Only one, Courellis et al., has studied freely moving marmosets moving in their environment[52,53]. Courellis et al. looked to analyze the relationship between theta oscillations and place cell activity in the common marmoset during a free moving task on a track. In this study, two marmosets were implanted with brush arrays in the anterior HPC, predominantly covering the DG and CA3, with some coverage in CA1. The group demonstrated the existence of theta bouts during the animals' movement, in contrast to continuous theta oscillations in the rat[41], and similar to previous macaque studies suggested that there may be some degree of bout-based theta phase coding in NHP HPC function[54]. They also outlined that theta was

not significantly modulated by movement (speed or direction), nor was consistently coupled with place cell activity. However, this study restricted the marmoset's movement to a linear track, only allowing movement in a single axis. The authors identify this as a means of comparison with rat research (which use a track), but this is a significant constraint. This is because marmosets are arboreal creatures, unlike rats, which move in all 3 planes as part of their natural movement including climbing, jumping and are uncomfortable remaining on the ground.

This begs the question, what is the observed modulation of LFPs in the marmoset's HPC when permitted to move freely in its environment, including the vertical plane?

In this thesis we aim to outline the modulation of LFP activity in the freely moving marmoset, comparing locomotion factors such as plane of motion and speed, with comparisons to the animal at rest for a prolonged period.

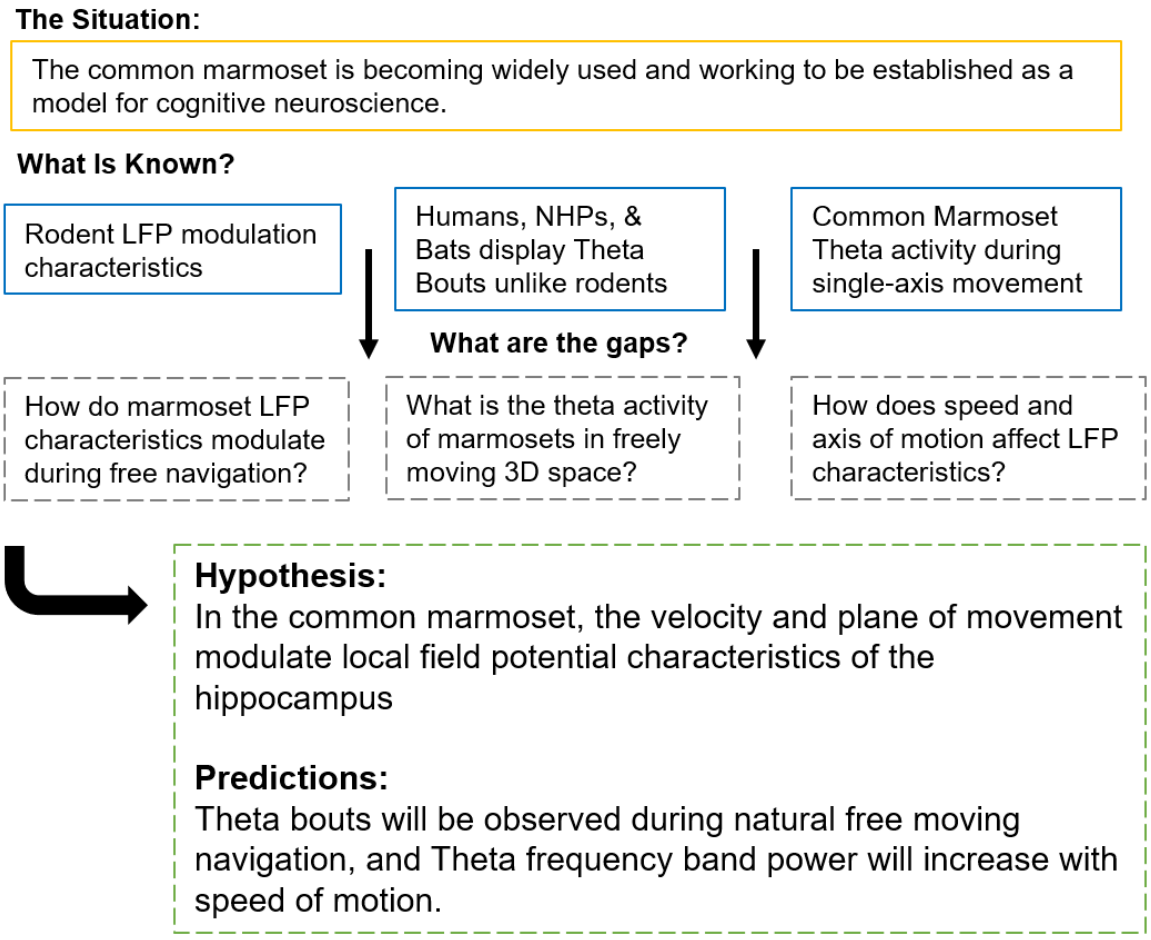


**Figure 3.** Hypothesis and predictions.

## 1.3 Hypothesis

In the common marmoset, the velocity and plane of movement modulate local field potential characteristics of the hippocampus.

## 1.4 Prediction

Theta rhythms will be seen in bouts and demonstrate greater amplitude during movement in comparison to stationary periods.

# Chapter 2

# 2 Methods and Materials

## 2.1 Animal Handling & Husbandry

All experimental procedures were approved by the University of Western Ontario Animal Use Subcommittee, University Council on Animal Care in accordance with the Canadian Council on Animal Care guidelines, and the Ontario Animals for Research Act. Studies were conducted with approved protocol 2020-137 for experimental work (Appendix A). Marmosets were housed in colony cages measuring 204 cm x 73 cm x 94 cm. Animals selected for recording were partnered with a cage-mate and placed in a separate housing cage (2 per cage) to minimize disruption of other marmosets. The relative humidity of the colony room was 30% - 70%, and temperatures approximately 24 C°, +/-3 were maintained, with a regular diurnal lightning cycle established. Marmosets were provided with daily dietary environmental enrichments (e.g., applesauce and acacia gum) during weekdays. The room was regularly cleaned by hosing down with lukewarm water, and daily removal of debris. Water was available for the animal as desired (ad libitum). Water quality was regularly monitored to ensure the absence of infectious or chemical contaminants. Standard base diets (Labdiet 5LK7 and 5040) with protein and fruit (e.g., boiled egg, shredded chicken, fruits, cereals, and nuts) were provided twice daily with food leftovers removed at each feeding.

Recording sessions were conducted in a separate area outside of their home cage room in a designated experimental suite. Transfers were made via a plexiglass transfer box draped with opaque cloth concealing the box during movement between locations.

## 2.2 Common Marmoset Data Set

### 2.2.1 Subjects

A total of two (n = 2) common marmosets (*Callithrix jacchus*) underwent array implantation, training, and recording in the dataset used for this thesis. These were comprised of one male, and one female subject. These animals were aged 3 and 4 years old, respectively, during the time of recording.

### 2.2.2 Acclimation Training

For months prior to implants, animals received acclimation training through daily handling. This would take a minimum of three weeks and progress from providing food-rewards through their home cage, to entering “transfer boxes”, to eventual physical handling. Once the animal was comfortable with the basics of trainer handling, they would begin training on their specific task (See Chapter 2.2.4). Once the animal was performing well and proving capable of the recording task, the marmoset underwent surgery.

### 2.2.3 Surgical Implants

Surgeries were conducted under the supervision of Dr. Julio Martinez-Trujillo in accordance with animal use protocol 2020-137. Surgeries were comprised of two parts: cap and array implants.

Marmosets were implanted with a cap made of a modular machine-fabricated polyether ether ketone (PEEK). This cap was comprised of three components including a base-ring, a spacer, and a lid. The base-ring was chronically adhered to the cleaned marmoset skull via UV-cured dental cement. The modular spacer was fastened to the ring via machine-screws, with spacer design selected for specifications related to the implant. Lastly the lid (made of 3-D-printed acrylonitrile butadiene (ABS)) was fastened to the base-ring via machine-screws. This lid was removed daily for access to the implant for recordings and cleanings. Dimples in the cap-spacer enabled head-fixation in the marmoset-chair[55] for cleaning and connecting the wireless recording stage (see Chapter 2.2.4).

Electrophysiological recording arrays used in both animals were achieved via brush arrays (Microprobes for Life Sciences, USA), and implanted in HPC CA1 & CA3 (Table 1, Figure 4). Arrays had 32-channels correlating to the 'brush' electrodes at the tip which would spread once inserted in brain-matter. Implants were achieved through a 1.5-2mm craniotomy, followed by the insertion of a medical-tubing cannula with associated metal stylet. Cannulas were inserted with a stereotaxic arm until 0.5-1.0 mm superior to the target tissue and cemented at the craniotomy with UV cured dental cement. Once the cannula was secured and the stylet removed, the electrode was inserted inside the cannula to the pre-determined depth. Sterilized silicone then sealed the implant area and remainder of the exposed skull. For Marmoset P, an additional component was a micro-driver (Rogue Research, Canada) which was fastened to both the array and the animal's skull. This additional mechanism enabled a semi-chronic implant for increasing the depth of the array deeper for use in future recording sessions, thus reaching fresh undamaged tissue.

| **Marmoset Name** | **Implant region** |
|---|---|
| Marmoset C | Posterior Left CA1 |
| Marmoset P | Anterior Right CA1/CA3 |

**Table 1.** List of marmoset implants used in this thesis.

Marmoset C's array was made with a chronic implant, while Marmoset P's was semi-chronic with the use of a micro-driver. Anterior vs posterior HPC function has been studied in humans, with the hippocampal encoding/retrieval and network (HERNET) model developed. This proposes that spatial encoding engages the anterior HPC, while retrieval engages the posterior HPC[56], which has been demonstrated in fMRI studies[57]. A human EEG study was also conducted to analyze theta oscillations between the anterior and posterior HPC, with results supporting the HERNET theory. However, as discussed in Chapter 1, both studies were in virtual paradigms rather than physical navigation. Our results (Chapter 3) and other work with this data set[58] show similar activity and function between the two animal regions, with the main variances between marmosets being movement plane preference.

### 2.2.4 Freely Moving Task

The freely moving task took place in a plexiglass environment comprised of 4 levels, with ropes to enable movement vertically between levels (Figure 4). Marmosets had both their body movements and neural activity recorded in real-time as they navigated through the environment. Body movement recordings were achieved through the Optitrack recording system, which is comprised of 14x infrared video cameras positioned 360 degrees around the animal. The body was tracked through reflective IR markers placed on the chronic headcap lid component, which allowed for software reconstruction of the areas of interest known as rigid bodies. These rigid bodies are tracked in 3-D space and allow for analysis of position, direction, and speed. The neurological data was wirelessly transmitted via the Blackrock Cereplex system. This operates via a wireless head stage connected to the array's omnetics connector transmitting to the receiving antennas. Together, these systems allow for the synchronous recording of the marmoset's position in space and accompanying cellular activity recordings. Recording sessions were an average of 40-60 minutes each in order to capture foraging behaviour.

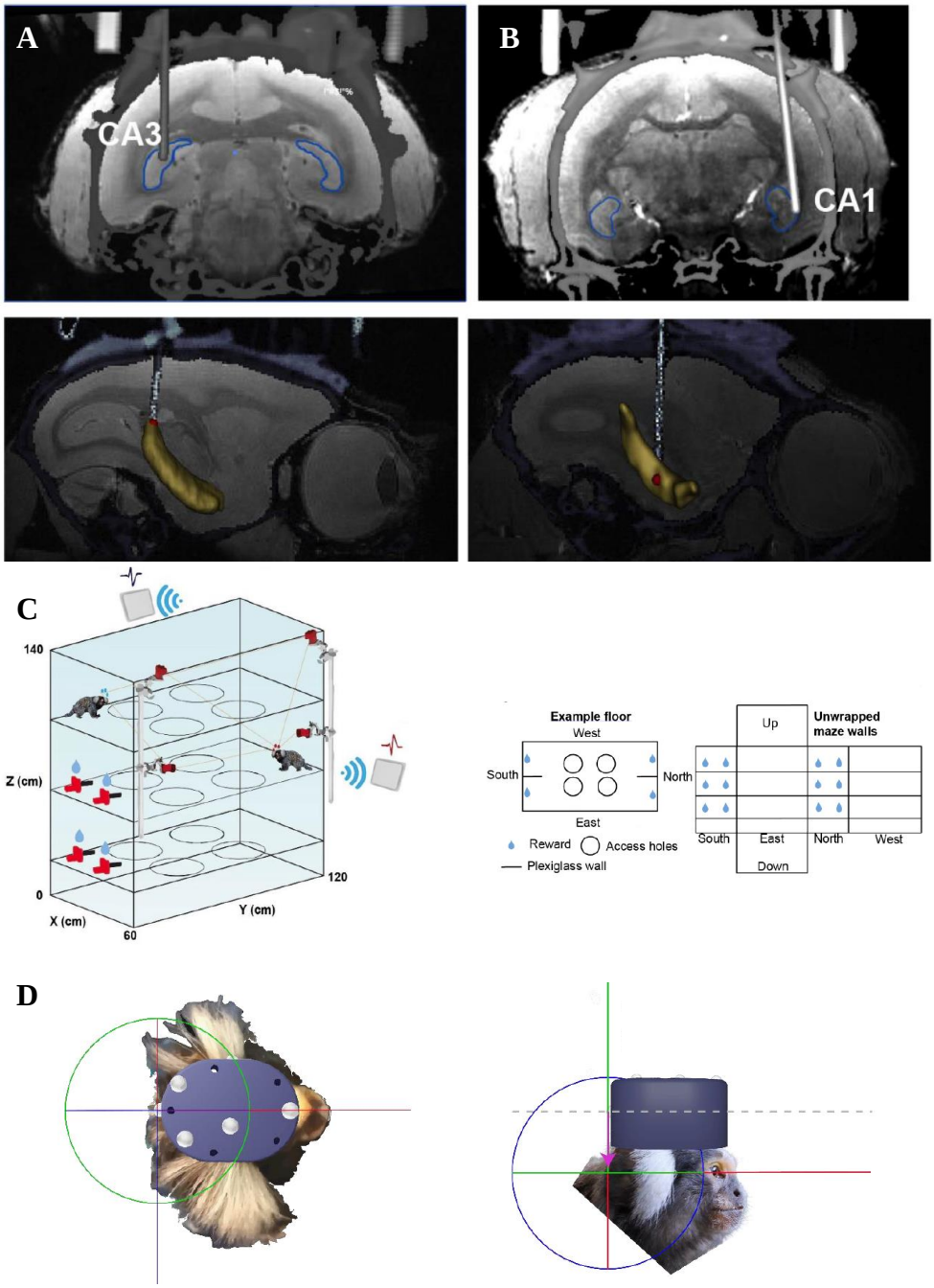


**Figure 4.** Implant verification scans and setup of recording apparatus.

Subfigures **A & B** visualize implants of Marmoset C and Marmoset P, respectively. MRI scans are placed as the base image, with confirmatory CT overlayed with bone shaded in colour (screws & dental cement from protective cap are also visible), and the marmoset HPC outlined in blue. In all quadrants the implanted array is visualized with the silver rod

in the structure. Marmoset C's implant was at the posterior tip of the left HPC, in the CA1 region. Marmoset P's implant was made in the right anterior CA1/CA3 region (difference in regions discussed in Table 1). HPC reconstructions can be seen in the lower images of both animals, with the hippocampus in gold, and the target site a red sphere. Subfigure **C** illustrates a graphic layout of the freely moving marmoset task. The plexiglass enclosure was 0.6m x 1.2m x 1.4m, comprised of 4 levels with holes in the floor, and rope which allowed the animal to move vertically through the environment. IR cameras and wireless antennas were placed surrounding the enclosure to record body movement and electrophysiological data, respectively. Three of the levels had ports for liquid reward with an accompanying LED light. LED lights were flashed, prompting the animal to move towards them, with rewards dispensed if the animal approached within 15cm of the location. Subfigure **D** shows an example of the location of the Optitrack reflective markers affixed to the head-cap which enable the recording system to track the animal's motion in 3-D space. Images courtesy of contributor DB.

## 2.3 Data Analysis

### 2.3.1 LFP Analysis of Freely Moving Marmosets

Neural datasets were recorded at 30kHz sampling rate and down sampled by the Blackrock Central software to 1kHz. Optitrack movement recordings were recorded at a sampling rate of 60Hz with recordings comprised of location in the x, y, and z planes. All analyses were processed in MATLAB by Mathworks, with the NPMK toolbox by Blackrock Neurotech for neurological recordings.

#### 2.3.1.1 Establishment of Movement Plane Epochs

First, X, Y, and Z positional data was converted from Optitrack CSS to MATLAB .mat format for processing. Positional data in metres was converted to speed at the sampling rate in cm/sec and paired to the Blackrock recording time (established by connection between Optitrack and Blackrock hardware with sync pulses pushed from the neural signal processor). X and Y movements were grouped together with overall horizontal speed determined by establishing the Euclidean norm (movement vector) via root sum of squares, while Z plane movement remained independent.

$$\text{RSS (Euclidean Norm)} = \sqrt{\sum_{i=1}^{n} \sigma_i^2}$$

Horizontal movement was binned in 500ms epochs based on the movement speed of the marmoset, then broken up into low and high speed. Low speed was set at 5cm/s which was determined as the lowest threshold of meaningful movement of animals being recorded, with high speed at 20cm/s and greater (Figure 5). This threshold of 20cm/s was independently determined for this thesis, but also match the speed threshold found in other marmoset & rodent LFP studies[52,59]. Horizontal epochs were contingent on both horizontal (XY plane) movement meeting the required meaningful speed threshold, while vertical movement (Z axis) remained below the 5cm/s threshold, isolating periods where the animal remained mobile in the horizontal plane. In cases where continuous movement was greater than 500ms, multiple epochs were binned per movement period (e.g. 3x 500ms epochs in a 1600ms movement period). Vertical speed was binned in 333ms epochs due to the very short duration of this movement classification (insufficient number of epochs lasting 500ms), and only applied in the high-speed movements (> 20cm/s). Vertical movement was subdivided by up and down movement, separating climbing/jumping ascents and descents. Lastly, stationary periods were defined as having 2,000ms of non-significant movement before and after the 500ms analysis window (total period of 4,500ms stationary). This was done to ensure the absence of possible LFP activity associated with anticipatory movement and planning.

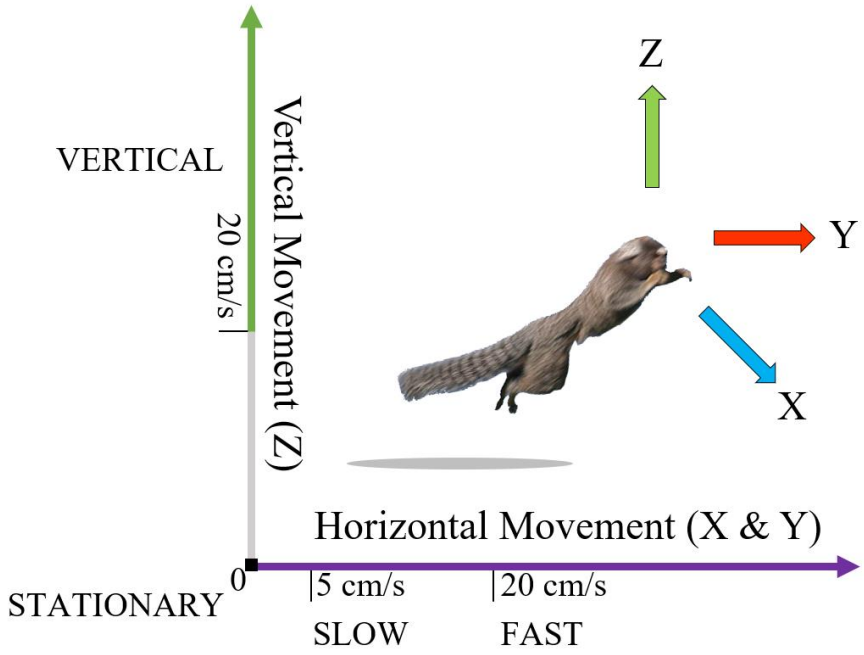


**Figure 5.** Categorization of movement speeds during freely moving task.

Animals were able to move freely in 3 dimensions (X,Y,Z) in the recording apparatus. These were broken into the horizontal (XY) and vertical (Z) planes. Speed was calculated in cm/s, with a threshold of 5cm/s for meaningful movement. In the horizontal plane, movement was sub-divided into slow (5cm/s – 20cm/s) and fast (> 20cm/s). Vertical movement was categorized as up or down, and above 20cm/s. The stationary condition was isolated for a 4.5s period of non-meaningful movement in any axis[60].

### 2.3.1.2 Neural Data Filtering

With movement epochs established, neural data was filtered to meet several quality checks to ensure meaningful LFP data (Figure 7). First, to remove common noise across channels, raw recorded data is converted to referenced data by subtracting the median of data across channels. Signal median was chosen instead of mean to mitigate the effect of outliers on noise removal. Epochs containing neural signal dropouts were detected with a 2ms threshold. If over 25% of channels during a recording session possessed the same flat signal across 2ms, that specific sample was flagged as too flat and discarded.

Fast Fourier Transform was applied per channel to filtered data (32 channels per session) returning a Fourier decomposition of time-series data, and the positive frequency values to which these were applied. These have also been demeaned with DC (0 Hz) removed from the data. This process enabled the isolation of frequency components of a signal and their contributory power to the sample (Figure 6).

$$Y(k) = \sum_{j=1}^{n} x(j) W_n^{(j-1)(k-1)} \text{ where } W_n = e^{(-2\pi)/n}$$

The magnitude of the Power Spectral Density (PSD) is then calculated by finding the mean-squared value of time-series data. Followed by converting to logarithmic decibels (dB).

$$dB = 10log_{10}\left(\frac{1}{n}\sum_{n=1}^{n} x_n^2\right)$$

With this decibel data, a line of best fit is estimated against the logarithmic frequencies from 2Hz to 55Hz. This upper value is used to remove influence of the 60Hz alternating current found in the Canadian electrical-infrastructure and detected by neural recordings. This line of best fit is calculated through a least-squares linear regression model.

$$a_1 = \frac{n\sum_{i=1}^{n} x_i y_i - (\sum_{i=1}^{n} x_i)(\sum_{i=1}^{n} y_i)}{n\sum_{i=1}^{n} {x_i}^2 - (\sum_{i=1}^{n} x_i)^2} \quad a_0 = \frac{(\sum_{i=1}^{n} y_i) - a_1(\sum_{i=1}^{n} x_i)}{n}$$

Channels with power spectral density slopes ($a_1$) steeper than -14 were eliminated. This is based off the principle that neural signals possess what are known as a pink-noise profile in their logarithmic PSD plots, with an ideal slope of 1/f (or -10 dB/decade). PSD profiles with slopes steeper than this encroach on Brownian noise ($1/f^2$ or -20 dB/decade) which is non-neuronal and characteristic of channels with non-LFP recordings and composed primarily of signal noise.

The result is neural data which is median-referenced for minimized noise, a slope proximal to 1/f, and free of dropouts or flat signals during 500ms epochs based on movement planes of specific speed categories (Figure 7). To establish slope referenced PSD profiles, the line of best fit calculated above was subtracted from the log-PSD

values, providing the delta value between the two. This isolated the LFP activity during the movement dependent condition from the overall profile of the PSD which is highly influenced by power-decay, as well as the nuances between recording sessions. This established referenced PSD allows for isolated comparative analysis of LFP profiles.

To effectively isolate LFP profiles, comparative analyses used referenced PSD maximums. To achieve these, the delta-log PSD made from subtracting the life of best fit from the log-PSD were converted back to power, and the maximum power found per frequency band, per channel were taken. This established the frequency's greatest positive deviation of power from the slope of the signal during the movement condition, and thus can contrast power relative to the other frequency bands during that condition.

$$power = 10^{(\frac{\Delta dB}{10})} \text{ where } \Delta dB = dB_n - (a_1 * n + a_0)$$

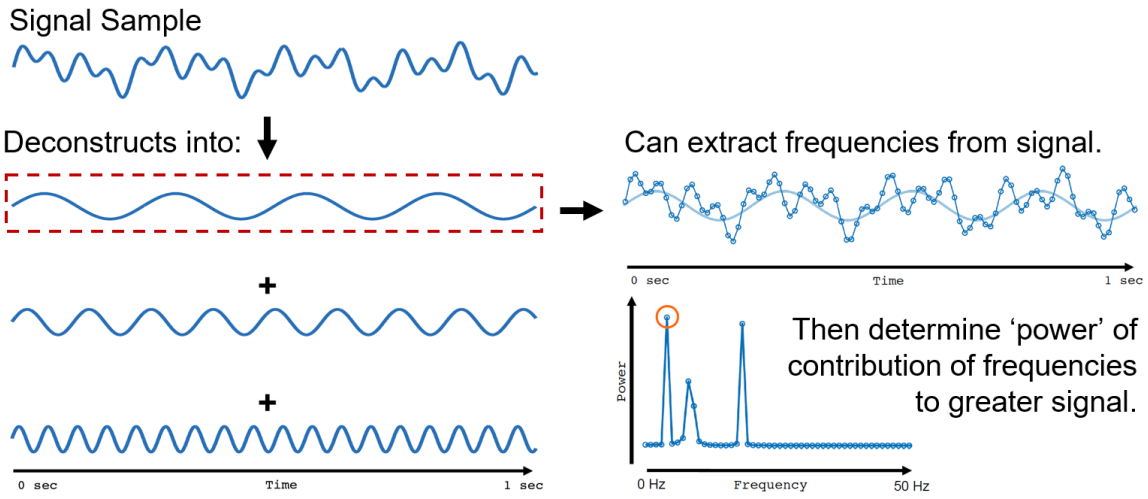


**Figure 6.** Theory behind LFP analysis.

Any recorded oscillatory signal is comprised of several different sinusoidal frequencies, which in combination make up the signal of interest. These frequencies are extracted via the Fourier Transform and can be quantified to determine their 'power' or relative contribution to the source signal. In this context, it is used to deconstruct neuro-oscillatory signal into its corresponding frequencies, which are grouped under frequency bands, e.g. theta at 4-8Hz[61].

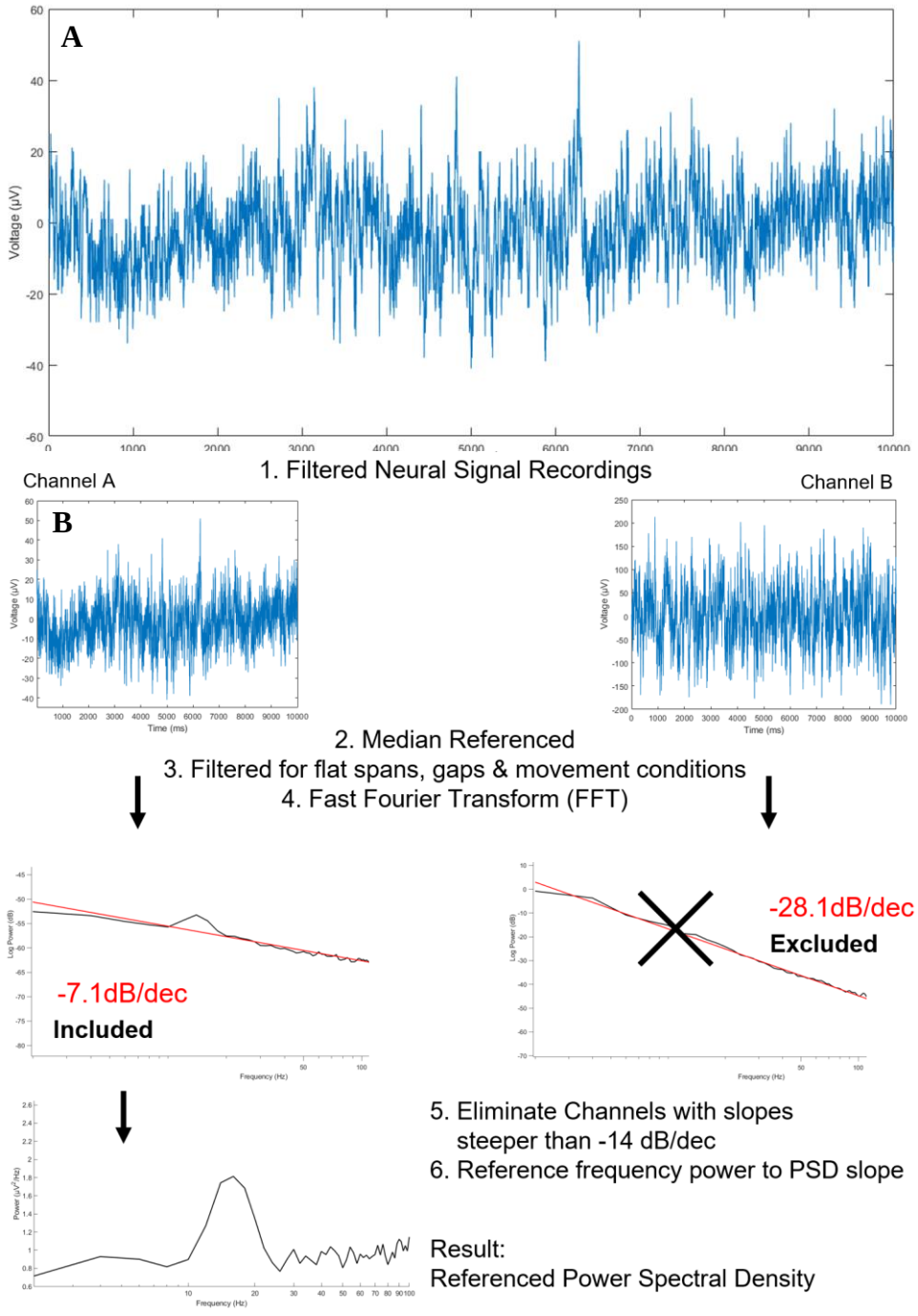


**Figure 7.** Data processing pipeline.

**A.** Visualized signal from freely moving condition in the marmoset HPC CA1 Region down sampled to 1kHz and a lowpass filter of 250Hz. **B.** Electrode array recordings are filtered to remove noise and signal drop (gaps or flat points). They are then binned

according to the animal's movement plane and velocity and processed by the Fast Fourier Transform (FFT). The subsequent logarithmic power spectral density (PSD) has its slope calculated via a least-squares linear regression model. The ideal 'pink noise' slope is 10 dB/dec, any channels with slopes steeper than 14 dB/dec are excluded. The data is converted to power and referenced to its slope, creating a condition-comparable PSD of power across frequencies. This result is used for subsequent LFP modulation analysis.

#### 2.3.1.3 Theta Bout Analysis

Theta bout analyses were achieved by creating a moving window FFT across an epoch period. This was done by isolating 1000ms epochs during the horizontal (slow & fast) and stationary conditions for each animal. This period was sampled every 5ms creating 101 windows. Each of these had the FFT discussed prior applied to them, enabling a series of PSDs depicting the change in frequency modulation every 5ms during a 500ms period. To isolate for theta bouts, bouts were defined as a continuous period of 80ms or greater where PSD values are at least 80% of the maximum value in the window for that period. Bouts were analyzed per channel, per epoch, and averaged across all values within a movement condition.

### 2.3.2 Statistical Analysis

All statistical analyses were done via MATLAB built-in statistical functions. Significance within a movement or frequency condition was determined by use of one-way ANOVA test. Subsequent multiple comparison test was completed via Tukey-Kramer test to produce pairwise significance values (p) across the different conditions within the group.

$$SE_{\bar{Y}_A-\bar{Y}_B} = \sqrt{\frac{MS_{within}}{n}} \quad \text{where } MES_{within} = \frac{\sum_{i-1}^{k}\sum_{j-1}^{n_i} Y_{ij}^2 \; - \; \sum_{i=1}^{k}(T_i^2/n_i)}{n-k}$$

Significance was defined if the determined p value was less than 0.05, with figure asterisks correlating to degree of significance corresponding to 0.05 > p > 0.01 (*), 0.01 > p 0.001 (**), and 0.001 > p (***). Scatter plot figures are plotted with subject mean and accompanying 95% confidence intervals.

# Chapter 3

# 3 Results

## 3.1 LFP Modulation Characteristics During Movement

As outlined in Chapter 2 (Methods), neural signal and movement recordings were isolated for periods based on the speed of movement of the animal. The marmosets' movements were separated in the horizontal plane (X,Y), and Vertical axis (Z), enabling the isolation of the animal performing lateral movement (running) and vertical movement (jumping/climbing). Recording sessions selected for analysis were only those that possessed both viable movement and neural recordings. Marmosets C and P had 22 and 25 recording sessions, respectively. Table 2 outlines the data yield extracted from the data set of the two animals. Worthy of note is the difference in movement tendencies between Marmoset C and P, where Marmoset C demonstrated an increased preference for vertical movement, while Marmoset P preferred horizontal movement. This plane of motion bias can be seen in the results with Marmoset C having greater error in horizontal movement, and Marmoset P having notable error in vertical movement resulting in globally higher power values (as seen in Figures 8B & 9B).

Power spectral density (PSD) plots were developed from these binned data sets, demonstrating the profile with 95% confidence interval of LFP activity in the 3-100 Hz range (Figure 8). These plots resulted in data with large confidence intervals likely resulting from variable recording conditions day-to-day along with the degradation of recording quality over the months of recording due to tissue granulation[62] which causes a change in the slope of LFP profile (Figure 7). Although useful to permit the visualization of LFP PSD which is standard, it does not provide a useful means of comparison across movement conditions as each PSD has confidence intervals overlapping as much as 100%. This means of analysis is also not effective for the proper comparison between frequency bands due to the nature of power law. This principle results in the phenomenon where power will decay proportionally as frequency increases (hence pink noise's profile of 1/f). The consequence of this is that power within the theta band (4-8 Hz) will

disproportionately be the greatest power in the spectrum, as it is the lowest frequency of interest, rather than relative to the PSD profile.

To address this, referenced PSD profiles (Chapter 2.3.1.2) were used to remove the large variability seen in the PSDs, making the data independent of the variable factors as previously discussed. These referenced PSDs (Figure 9A & 9B) illustrate the variation of LFP power across the frequency spectrum without the limitation of power-law and recording variability. By visually flattening data through a histogram (Figure 9C & 9D) a clearer comparison of normalized mean LFP power across movement conditions is seen. This histogram suggests that slow moving (stationary and both horizontal-slow) movement conditions have similar LFP profiles with a concentration of the greatest power at the 8Hz band. In contrast, vertical movement sees this elevated power at 10Hz (alpha frequency), and horizontal-fast showing frequency power characteristics of both horizontal-slow and vertical conditions.

One limiting factor observed in these results is the profile of the vertical movement due to the rapid speed of vertical motion. The isolation of horizontal movement periods allowed for high yield of 500ms periods due to the size of the recording enclosure. In contrast, vertical movement is explosive and occurs rapidly, requiring a maximum of 333ms epochs. This resulted in a notable difference in the number of vertical movement epochs per recording session, subsequently creating larger confidence intervals and jagged profile (Figure 8A & 8B). A consequence of having a smaller sample window for the vertical conditions is the FFT outputting power in larger frequency parcels, which in-part contribute to the more jagged shape seen in the vertical movements in Figure 9.

With Ref-PSD profiles established we looked to draw observations across frequency bands (e.g. theta 4-8Hz). This revealed the problem with using power means across frequencies. The result was that the alpha band (8-12Hz) was consistently the highest power output rather than the frequency band which saw the largest spike in activity (Figure 10). To correct for this, referenced PSD maximums were used draw comparisons across frequencies (defined as greatest deviation from the PSD slope per channel, per epoch (Chapter 2.3.1.2)).

With movement condition and frequency band maximums, comparisons could be made of LFP modulation based on marmoset movement (Figure 11, Table 3). Extrapolating from frequency bands across movement conditions (Figure 11B & 11D), theta (4 to 8 Hz) remains the greatest power during slow movement periods (stationary and horizontal-slow), subsequently moving to the weakest power as speed and complexity of motion increases. Beta (14 to 30 Hz) shows the inverse relationship, starting as the smallest power when the animal is stationary and becoming the strongest with vertical movement. This relationship is also seen when comparing movement conditions to frequency bands (Fig 11A & 11C), where Marmoset C displayed similar theta power between non-rapid (stationary and horizontal-slow) and vertical motion, but this relationship significantly changed with vertical motion power becoming significantly greater in the beta band.

Due to the movement bias between animals, care must be taken when comparing horizontal and vertical motion. An example of this is the relationship between vertical up and down movement. These two animals show inverse relationships between the two movements, but Marmoset C has 13 times more recording samples included in its vertical-down yield, which would suggest this relationship is closer to the true population. This is a result of using LFP maximums which use means of the greatest deviation from the PSD slope. Smaller sample sizes will have proportionally higher values, creating an additive effect with overall power and values creeping upwards[63]. This is apparent in the size of error bars and spread of data which is well illustrated in Figure 11D where Marmoset P's sample size decreases moving across the figure's x axis.

| | Number of Sessions | Channel Count | Mean Channels Per Epoch | Stationary | Horizontal-Slow | Horizontal-Fast | Vertical-Up | Vertical-Down |
|---|---|---|---|---|---|---|---|---|
| | | | | **Number of Epochs** | | | | |
| Marmoset C | 22 | 1218 | 28 | 4,673 | 953 | 195 | 170 | 298 |
| Marmoset P | 25 | 1222 | 24 | 17,674 | 1,819 | 370 | 56 | 24 |
| | | | | **Total Samples** (Epoch x Channels per Session) | | | | |
| | | | | 135,972 | 27,595 | 5,506 | 4,318 | 8,145 |
| | | | | 455,289 | 44,912 | 9,439 | 1,259 | 613 |

**Table 2.** Data yield of LFP modulation analysis.

Data yield for LFP modulation analysis from data set. Channel count is defined as the sum of viable channels across all recording sessions, with the mean being the average number of viable channels per session. Number of epochs are the total number of epochs per animal across all recording sessions for the specific movement condition. Total samples are the statistical n value used during analysis and are the result of the sum of epochs multiplied by the number of viable channels which recorded the epoch.

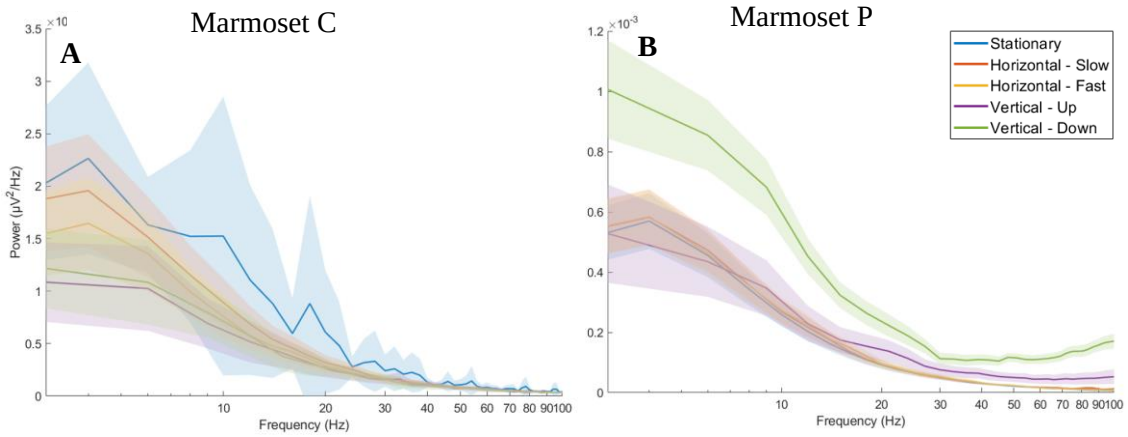


**Figure 8.** Power Spectral Densities during movement conditions.

Power spectral density profiles of Marmoset C (**A**), and Marmoset P (**B**) across all recording sessions and channels. PSD profiles are derived from neural data during specific movement conditions. These being stationary (Blue), horizontal-slow (5cm/s-20cm/s) (Orange), horizontal-fast (20cm/s+) (Yellow), vertical-up (movement purely in the vertical plane upwards) (Purple) and lastly vertical-down (movement purely in the vertical plane downwards) (green).

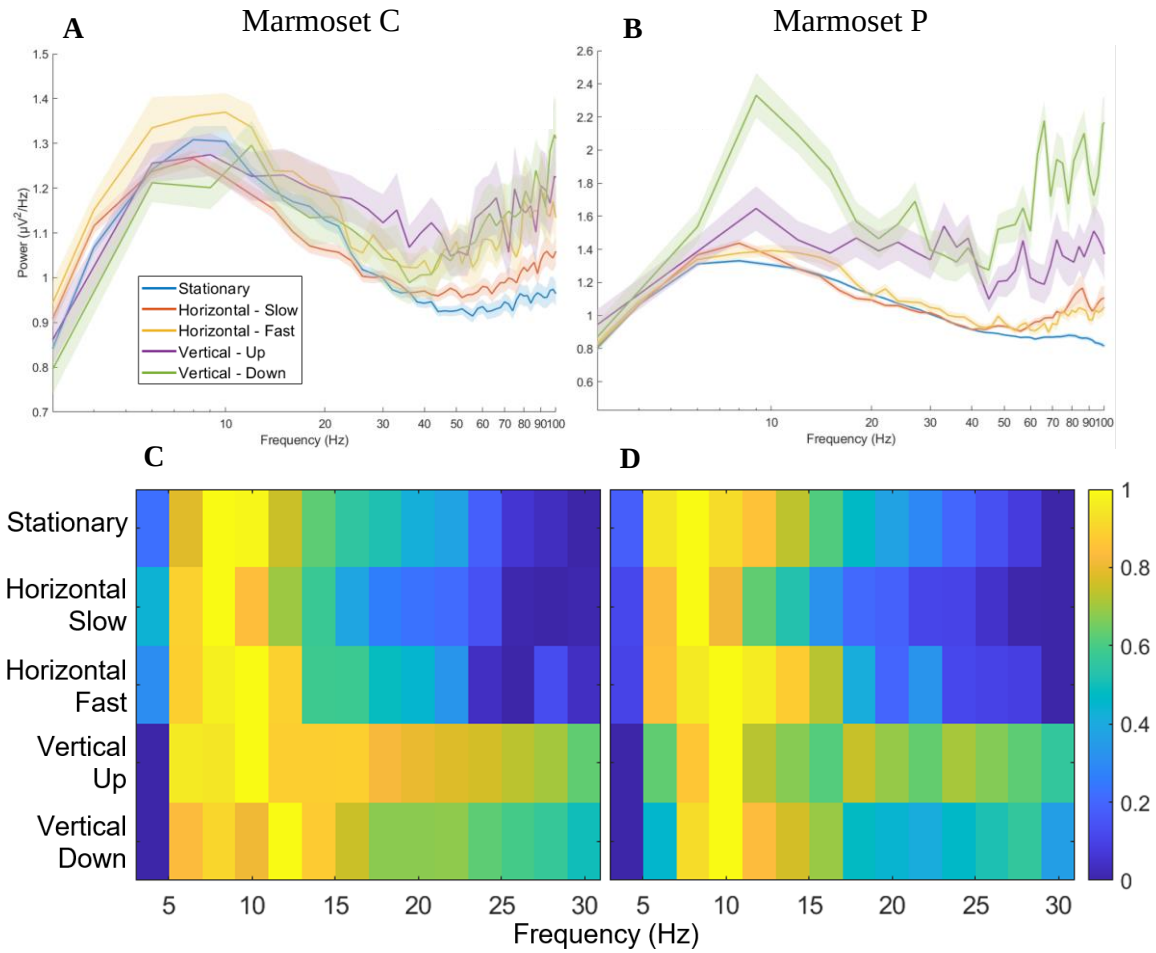


**Figure 9.** Referenced power spectral density plots of movement conditions.

Referenced power spectral density plots of Marmoset C (**A**) and Marmoset P (**B**). These referenced PSDs are segmented by movement plane condition (same as Figure 8). The trends can be visualized clearly on histograms **C** and **D** for Marmosets C & P, respectively. Data outlined in histograms are 'range' normalized such that the highest value is 1, and lowest 0.

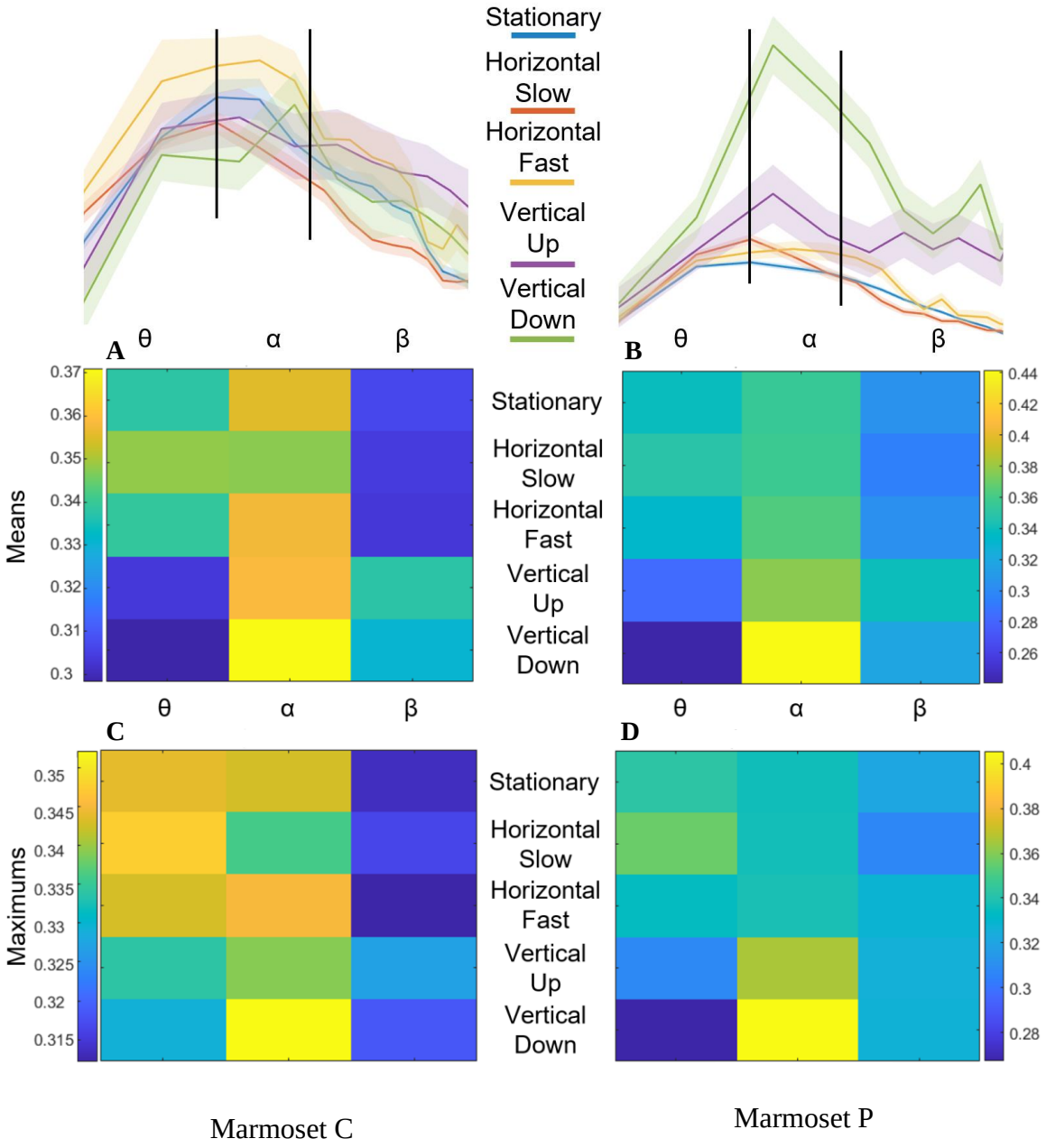


**Figure 10.** Difference in analysis profile between mean and maximum frequency bands.

Difference in analysis profile between mean and maximum frequency bands. Subfigures **A** and **B** illustrate the outcome of analysis based on frequency band means, while Subfigures **C** and **D** show the more relevant profile achieved by analyzing frequency maximums which allows for visualizing LFP fluctuations.

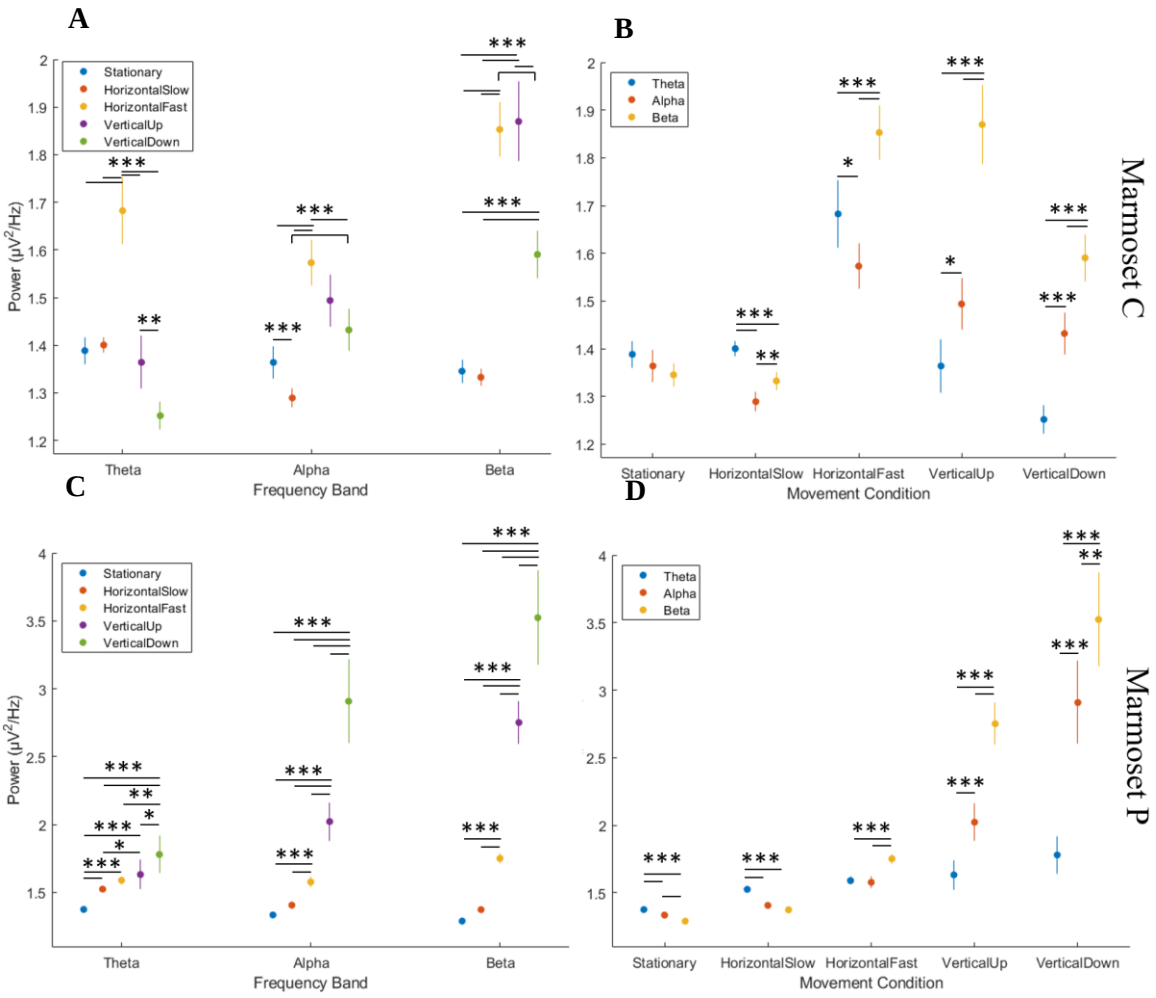


**Figure 11.** Modulation of LFP frequency band maximums during movement conditions.

Subfigures **A** and **C** illustrate a comparison of mean LFP power maximums of movement conditions based on frequency bands for Marmosets C and P, respectively. Subfigures **B** and **D** show a comparison of LFP power maximums between frequency bands based on the movement condition it was expressed in. Statistics for significance between points are outlined in Table 3.

| Marmoset C | θ | | | | | α | | | | | β | | | | |
|---|---|---|---|---|---|---|---|---|---|---|---|---|---|---|---|
| | Stationary | Horizontal-Slow | Horizontal-Fast | Vertical-Up | Vertical-Down | Stationary | Horizontal-Slow | Horizontal-Fast | Vertical-Up | Vertical-Down | Stationary | Horizontal-Slow | Horizontal-Fast | Vertical-Up | Vertical-Down |
| Stationary | | p = 0.99 | p < 0.001 | p = 0.95 | p < 0.001 | | p = 0.06 | p < 0.001 | p < 0.001 | p = 0.14 | | p = 0.99 | p < 0.001 | p < 0.001 | p < 0.001 |
| Horizontal-Slow | p = 0.99 | | p < 0.001 | p = 0.80 | p < 0.001 | p = 0.06 | | p < 0.001 | p < 0.001 | p < 0.001 | p = 0.99 | | p < 0.001 | p < 0.001 | p < 0.001 |
| Horizontal-Fast | p < 0.001 | p < 0.001 | | p < 0.001 | p < 0.001 | p < 0.001 | p < 0.001 | | p = 0.06 | p < 0.001 | p < 0.001 | p < 0.001 | | p = 0.99 | p < 0.001 |
| Vertical- Up | p = 0.95 | p = 0.80 | p < 0.001 | | p = 0.009 | p < 0.001 | p < 0.001 | p = 0.06 | | p = 0.27 | p < 0.001 | p < 0.001 | p = 0.99 | | p < 0.001 |
| Vertical-Down | p < 0.001 | p < 0.001 | p < 0.001 | p = 0.009 | | p = 0.14 | p < 0.001 | p < 0.001 | p = 0.27 | | p < 0.001 | p < 0.001 | p < 0.001 | p < 0.001 | |

| | Stationary | | | Horizontal-Slow | | | Horizontal-Fast | | | Vertical-Up | | | Vertical-Down | | |
|---|---|---|---|---|---|---|---|---|---|---|---|---|---|---|---|
| | θ | α | β | θ | α | β | θ | α | β | θ | α | β | θ | α | β |
| θ | | p = 0.48 | p = 0.11 | | p < 0.001 | p < 0.001 | | p = 0.029 | p < 0.001 | | p = 0.017 | p < 0.001 | | p < 0.001 | p < 0.001 |
| α | p = 0.48 | | p = 0.66 | p < 0.001 | | p = 0.003 | p = 0.029 | | p < 0.001 | p = 0.017 | | p < 0.001 | p < 0.001 | | p < 0.001 |
| β | p = 0.11 | p = 0.66 | | p < 0.001 | p = 0.003 | | p < 0.001 | p < 0.001 | | p < 0.001 | p < 0.001 | | p < 0.001 | p < 0.001 | |

| Marmoset P | θ | | | | | α | | | | | β | | | | |
|---|---|---|---|---|---|---|---|---|---|---|---|---|---|---|---|
| | Stationary | Horizontal-Slow | Horizontal-Fast | Vertical-Up | Vertical-Down | Stationary | Horizontal-Slow | Horizontal-Fast | Vertical-Up | Vertical-Down | Stationary | Horizontal-Slow | Horizontal-Fast | Vertical-Up | Vertical-Down |
| Stationary | | p < 0.001 | p < 0.001 | p < 0.001 | p < 0.001 | | p = 0.63 | p < 0.001 | p < 0.001 | p < 0.001 | | p = 0.57 | p < 0.001 | p < 0.001 | p < 0.001 |
| Horizontal-Slow | p < 0.001 | | p = 0.23 | p = 0.03 | p < 0.001 | p = 0.63 | | p = 0.009 | p < 0.001 | p < 0.001 | p = 0.57 | | p < 0.001 | p < 0.001 | p < 0.001 |
| Horizontal-Fast | p < 0.001 | p = 0.23 | | p = 0.78 | p = 0.002 | p < 0.001 | p = 0.009 | | p < 0.001 | p < 0.001 | p < 0.001 | p < 0.001 | | p < 0.001 | p < 0.001 |
| Vertical- Up | p < 0.001 | p = 0.03 | p = 0.78 | | p = 0.017 | p < 0.001 | p < 0.001 | p < 0.001 | | p < 0.001 | p < 0.001 | p < 0.001 | p < 0.001 | | p < 0.001 |
| Vertical-Down | p < 0.001 | p < 0.001 | p = 0.002 | p = 0.017 | | p < 0.001 | p < 0.001 | p < 0.001 | p < 0.001 | | p < 0.001 | p < 0.001 | p < 0.001 | p < 0.001 | |

| | Stationary | | | Horizontal-Slow | | | Horizontal-Fast | | | Vertical-Up | | | Vertical-Down | | |
|---|---|---|---|---|---|---|---|---|---|---|---|---|---|---|---|
| | θ | α | β | θ | α | β | θ | α | β | θ | α | β | θ | α | β |
| θ | | p < 0.001 | p < 0.001 | | p < 0.001 | p < 0.001 | | 0.88 | p < 0.001 | | p < 0.001 | p < 0.001 | | p < 0.001 | p < 0.001 |
| α | p < 0.001 | | p < 0.001 | p < 0.001 | | p = 0.10 | 0.88 | | p < 0.001 | p < 0.001 | | p < 0.001 | p < 0.001 | | p = 0.0063 |
| β | p < 0.001 | p < 0.001 | | p < 0.001 | p = 0.10 | | p < 0.001 | p < 0.001 | | p < 0.001 | p < 0.001 | | p < 0.001 | p = 0.0063 | |

**Table 3.** Statistical significance of modulation of LFP frequency band maximums during movement conditions.

Tables outlining the statistical significance of LFP power comparisons seen in Figure 11. Values that are highlighted in green are of statistical significance ($p < 0.05$) according to one-way ANOVA and subsequent Tukey-Kramer test (Chapter 2.3.2).

## 3.2 Theta Bouts During Horizontal Movement

To isolate and visualize the pattern of theta band frequency activity during movement, 500ms periods were isolated and analyzed during horizontal and stationary movement conditions (Chapter 2.3.1.3). An example of these theta bouts can be seen in Figure 12, which are characterized by temporary periods of high theta-band activity relative to other frequencies during the animal's movement. Characterization of the theta bouts was completed to determine the frequency and duration of theta bouts during movement conditions (Figure 13). There was a significant increase for both animals in theta bouts during horizontal-fast condition in comparison to when the animal was stationary. In marmoset C there was also significantly more theta bouts during horizontal-fast versus horizontal-slow movement.

Length of theta bouts were calculated with no significant variation seen, although a downward trend is apparent. Data profile of bout lengths show that group medians were similar to the mean, with a gaussian distribution. Similar to the limitation of vertical values during the LFP modulation analysis, due to the length of time required to capture theta bouts (1,000ms window for 500ms analysis period) the number of horizontal-fast epochs was limited because the physical constraints of the recording environment resulted in fast bursts rarely last over a second (Table 4). This is best seen in Marmoset C, where over the period of 22 sessions the animal only performed six horizontal-fast movement bursts lasting over 1,000ms. As a result, the sample size is restricted, leading to larger confidence intervals and difficulty determining significance.

| | Number of Sessions | Channel Count | Mean Channels Per Epoch | Stationary | Horizontal-Slow | Horizontal-Fast |
|---|---|---|---|---|---|---|
| | | | | **Number of Epochs** | | |
| Marmoset C | 22 | 1218 | 28 | 1822 | 63 | 6 |
| Marmoset P | 25 | 1222 | 24 | 6396 | 235 | 29 |
| | | | | **Total Samples** (Epoch x Channels per Session) | | |
| | | | | 51666 | 1785 | 160 |
| | | | | 156930 | 4748 | 653 |

**Table 4.** Data yield of theta bout analysis.

Data yield for theta bout analysis from data set. Channel count is defined as the sum of viable channels across all recording sessions, with the mean being the average number of viable channels per session. Number of epochs are the total number of epochs per animal across all recording sessions for the specific movement condition. Total samples are the statistical n value used during analysis and are the result of the sum of epochs multiplied by the number of viable channels which recorded the epoch.

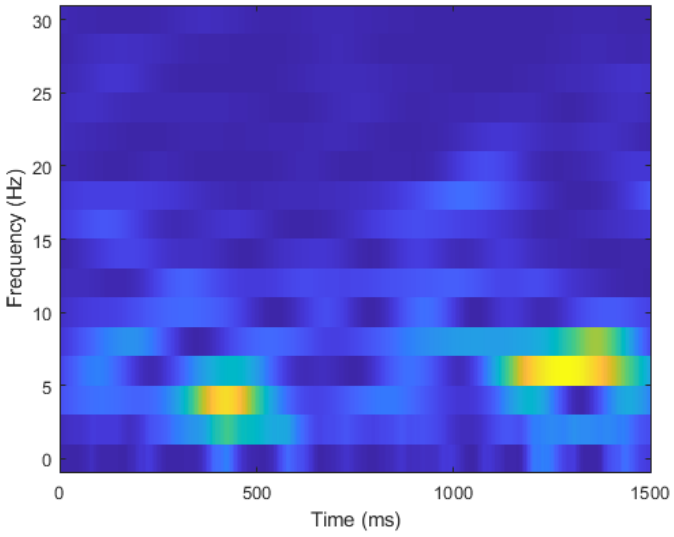


**Figure 12.** Example histogram of theta bouts.

Sample histogram of ‘theta bouts’ observed in Marmoset C during horizontal-slow movement as the animal moved from one side of the recording enclosure to another. Characterized by non-continuous bursts of LFP power in the theta frequency band (4-8Hz).

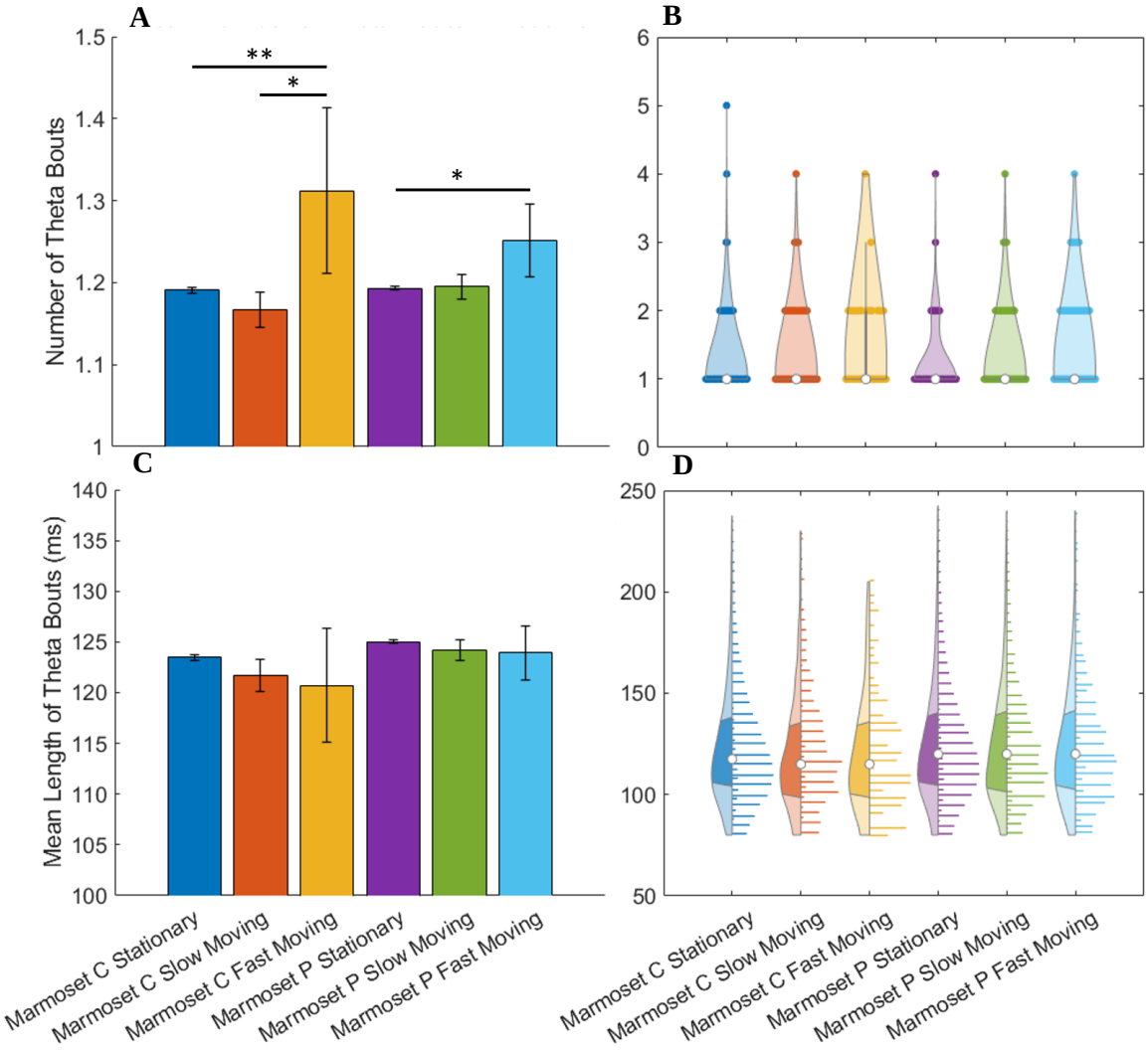


**Figure 13.** Analysis of the frequency, and length of theta bouts during horizontal movement in a 500ms period.

Subfigures on the left provide a bar-histogram of the mean values for the category, while the right subfigures provide a violin plot of the data to outline the spread and profile of the results. Subfigures **A** and **B** show the mean number of theta bouts during the movement condition epoch. Subfigures **C** & **D** outline the mean duration of theta bouts observed.

# Chapter 4

# 4 Discussion

This thesis aimed to investigate the observed LFP modulations in the marmoset HPC when given the ability to move freely in its environment. This was achieved in two stages. First, by analyzing of the modulation of frequency band power as the animal moved in five distinct movement conditions. Second, the examination of theta bout activity while the animal was at rest and in motion. Our major findings are that LFP profiles modulate based on both the speed and plane of movement of the animal, and that theta bouts are present in the naturally moving marmoset both at rest, and in motion.

## 4.1 Theta Power is Inverse to Movement Speed

Across both animals, theta band oscillations had the greatest power when compared to alpha and beta when at rest and during horizontal-slow movement. Current literature does not compare NHP LFP frequencies during movement. However, theta oscillations have shown their importance in spatial attention and environmental exploration, in the coined rhythmic theory of attention[64]. This theory is proposed that theta rhythms in attention networks resolve conflicts by organizing sensory and motor functions. In primates, this exploratory behaviour would be through gaze, specifically saccadic eye movement, which in NHPs and humans occur at a frequency of 2-3 saccades per second[48,65]. Although its exploratory sensor is visual like other NHPs, new-world primates, including the marmoset, prefer whole head movement to change its gaze, rather than via saccades[66,67], but are capable of making deliberate eye saccades to areas of interest[68]. In the freely moving marmoset it has been recently shown that exploratory head movements occurred 80% when stationary, and only 20% in motion, compared to the rat was is 14% and 86%, respectively[58]. From this, we suggested that theta oscillations are the prominent oscillation band during the stationary period due to this role in gaze exploration. Theta has also been shown to play a role in vestibular orientation in NHPs which would play a role during this exploratory phase[69].

When the animal moves through its environment, theta oscillations work in a non-continuous pattern known as bouts (discussed in Chapter 4.2). The link between theta

bouts and hippocampus function during navigation remains unclear. One possibility which has been recently proposed, is that they relate to the exploratory gaze movements animals make when freely moving[58]. Marmoset saccades/head movement frequency has not been previously reported, but if similar to other NHPs (2-3/sec), this would loosely correlate to the rate of theta bouts seen while the marmoset was stationary and moving (2-3 bouts/second). If this is the case, theta oscillations seem to differ in their role between marmosets and other species such as rats and mice, but this issue needs further investigation (Chapter 4.3).

With the increase in movement speed, beta power increased to become the prominent frequency band during rapid (vertical and horizontal-fast) movement. Beta oscillations are known for motor planning and providing information to the sensorimotor system to control motor output (Chapter 1.1). Although these functions do not originate in the HPC, the HPC remains part of a larger network receiving connections from those regions responsible (Figure 1). What is seen in our results is that with the increase in speed from stationary to vertical-down movement, beta oscillation power markedly increases, becoming significantly greater in the horizontal-fast and both vertical conditions. This correlation of speed and beta LFP power has also been reported in rodent models[70]. It is likely that as the speed and complexity of movement increases, the HPC receives greater sensory-motor input for use in navigation, prediction, and memory during the execution of this locomotion, resulting in the elevation of beta power recorded in the region.

Bridging these theories would suggest that theta oscillations are involved while the animal remains at rest and engaging in exploratory gaze behaviour. As the animal begins to move, the HPC begins to receive additional beta frequency inputs significantly increasing in power while theta also continues to climb. As the animal's movement increases in speed and complexity, the input of beta frequency continues to increase until its power significantly exceeds that of theta. A significant increase in theta power with speed was also exhibited in rats, but showed the inverse for higher frequencies which showed a reduction in power with speed[70].

## 4.2 Theta Bouts During Movement

In this thesis, the existence of theta bouts rather than continuous theta oscillations (as seen in the rodent model) was observed during both stationary and moving conditions. Observations during movement periods are inline with previous marmoset navigation literature, as well as those in NHP and human studies, while isolation of marmoset theta bouts during stationary periods has not been previously reported[45,52,71]. Our findings are in concurrence with previous literature in that the speed of the marmoset's movement did not have a significant impact on theta bouts during movement[52]. However, our results show a significant increase in theta bout frequency during horizontal-fast movement when compared to stationary. As discussed in Chapter 4.1, this may potentially be a result in the transition from theta as a function of visual exploration when stationary to movement navigation during motion.

These findings provide support to the theory that the existence of theta bouts is not due to experimental paradigms which prohibit natural animal motion (e.g. paradigms seen in previous human and NHP studies). Rather this along with findings in the fruit bat[42,43], suggest that the rodent hippocampal function has a different relationship to theta oscillations compared to the other models listed. Mankin et al. looked to investigate this discrepancy, comparing the rat to a rodent model which is diurnal with high visual acuity and low-frequency hearing like primates: the Mongolian gerbil. Their results showed that despite these sensory differences gerbils showed only minor differences in hippocampal activity, including the presence of continuous theta rhythms rather than bouts. They concluded that the differences seen between rodents and primates cannot be solely attributed to the specialization of the auditory and visual systems[72]. Comparing the findings across these 5 research models provide a compelling observation of the differences that exist between rodent and primate literature, and the need for more focused navigation and hippocampal research in primate models, for which the common marmoset would be well suited.

## 4.3 Limitations

A limitation of this thesis was the size and composition of subjects used. Only two common marmosets (n = 2) were used for this study. Although this is inline with other marmoset studies involving invasive implants[52,58], these two animals received implants in different locations (anterior and posterior HPC) and were of different sexes. This is potentially significant due to possible effects of implant location such as the HERNET theory (Table 1), and that previous studies have noted differences in neural activity during navigation between sexes[73,74]. This creates a variability between the two marmosets, limiting the ability to draw conclusions of differences in results as this would be confounding. Future studies should have an increased sample size with animals of the same sex and implant location, or proportionally sufficient sample size per variable between groups (e.g. two implant locations with an n-value of 2-3 of the same sex per location).

One of the greatest limitations found in this thesis was the sample size of the data collected. In addition to the limited n value, the relative scarcity of certain movement types placed constraints on statistical analysis. This predominantly affected rapid movements (horizontal-fast and vertical). Although the animals had the ability to move vertically through their environment, the behaviour recorded showed relatively limited number of vertical climbs or jumps, notably in Marmoset P with 1,819 horizontal-slow epochs compared to a collective 80 vertical (up and down). This limitation comes in part from the nature of the common marmoset being arboreal (and prey) creatures, the tendency is for them to remain at elevated heights with a reluctance/avoidance of descending to levels closer to ground unless necessary. A similar freely moving environment with interventions (e.g. level closing off forcing the animal to change their vertical position) would enable a greater number of vertical movement conditions for analysis. The same principle could be applied for horizontal-fast movement as seen by the limited number in Marmoset C. This created a scarcity of vertical movement epochs in Marmoset P, and horizontal-fast in Marmoset C, which limited the significance and potentially precision in comparison to the other movement types (can be seen in figures with size of comparable confidence intervals).

This movement limitation was also seen for the characterization theta bouts. This is a case where a longer more linear environment such those from previous studies would prove favourable as it could induce sufficient samples of rapid movement over sufficient distance. Additionally, no vertical theta bouts were analyzed due to the absence of any vertical motion lasting more than 500ms. A vertical enclosure with a rope or metal mesh would enable vertical motion to another level ensuring the existence of epochs of sufficient length. This would also allow for the differentiation of two forms of vertical-up movement, jumping and climbing, two natural forms of locomotion of the common marmoset. Predominantly the movement seen in this study were jumps made by the marmosets from level to level, but in an environment of sufficient height where jumping is not possible to reach the destination, this would force the animal to climb and achieve this second category of vertical movement.

In short, a replication of this study in more than one recording environment would enable a more in-depth and accurate analysis, enabling further characterization of the neural mechanics seen in both vertical and horizontal-fast movement. For example, one freely moving 3-D environment such as what was done here, and two more artificial environments which would enable observation of vertical and horizontal movement under more artificial conditions.

## 4.4 Novelty of Research Conducted

As previously discussed, only one published article by Courellis et al. looked at the LFP characteristics of freely moving common marmoset hippocampus. The constraint in this study was the restriction of the marmoset to a linear track in one plane of motion. This thesis looked at the modulation of theta rhythms of the freely moving marmoset in all 3 planes of motion, where the animal had the freedom of movement to choose their direction. We are the first to examine the comparative modulation of theta, alpha, and beta frequency bands in the hippocampus during a freely moving task. In addition, observed isolated stationary theta bouts in the common marmoset, and its comparison against movement conditions.

## 4.5 Conclusion

We have shown that when the common marmoset moves freely within 3-D space, there is observed modulation of LFP characteristics dependant on both the speed of movement and axis of motion in which the animal navigates. This thesis has also contributed to the limited existing literature on marmoset LFP studies, further defining the characteristics of its function namely the need for further research on vertical locomotion. These results have provided further evidence of the evolutionary departure of hippocampal LFP functions in NHP models from rodents, and that despite the large foundation laid by navigation research in the rodent model, the common marmoset shares greater similarities to NHPs and humans. This strengthens the case for the common marmoset in becoming the standard animal model used to understand primate navigation.

# References


1. Tatu, L. & Vuillier, F. Structure and vascularization of the human hippocampus. *Front Neurol Neurosci* **34**, 18–25 (2014).

2. Kesner, R. P. & Rolls, E. T. A computational theory of hippocampal function, and tests of the theory: New developments. *Neuroscience & Biobehavioral Reviews* **48**, 92–147 (2015).

3. Rolls, E. T. The storage and recall of memories in the hippocampo-cortical system. *Cell Tissue Res* **373**, 577–604 (2018).

4. Rolls, E. T. *Cerebral Cortex: Principles of Operation*. (Oxford University Press, 2016).

5. Azarfar, A., Calcini, N., Huang, C., Zeldenrust, F. & Celikel, T. Neural coding: A single neuron's perspective. *Neurosci Biobehav Rev* **94**, 238–247 (2018).

6. Corrigan, B. W. *et al.* Distinct neural codes in primate hippocampus and lateral prefrontal cortex during associative learning in virtual environments. *Neuron* **110**, 2155-2169.e4 (2022).

7. Hartley, T., Lever, C., Burgess, N. & O'Keefe, J. Space in the brain: how the hippocampal formation supports spatial cognition. *Phil. Trans. R. Soc. B* **369**, 20120510 (2014).

8. O'Keefe, J. Place units in the hippocampus of the freely moving rat. *Experimental Neurology* **51**, 78–109 (1976).

9. Savelli, F., Yoganarasimha, D. & Knierim, J. J. Influence of boundary removal on the spatial representations of the medial entorhinal cortex. *Hippocampus* **18**, 1270–1282 (2008).

10. Hafting, T., Fyhn, M., Molden, S., Moser, M.-B. & Moser, E. I. Microstructure of a spatial map in the entorhinal cortex. *Nature* **436**, 801–806 (2005).

11. Quiroga, R. Q. Gnostic cells in the 21st century. *Acta Neurobiol Exp (Wars)* **73**, 463–471 (2013).

12. Fox, K. C. R., Andrews-Hanna, J. R. & Christoff, K. The neurobiology of self-generated thought from cells to systems: Integrating evidence from lesion studies, human intracranial electrophysiology, neurochemistry, and neuroendocrinology. *Neuroscience* **335**, 134–150 (2016).

13. Buzsáki, G., Anastassiou, C. A. & Koch, C. The origin of extracellular fields and currents — EEG, ECoG, LFP and spikes. *Nat Rev Neurosci* **13**, 407–420 (2012).

14. Cobb, S. R., Buhl, E. H., Halasy, K., Paulsen, O. & Somogyi, P. Synchronization of neuronal activity in hippocampus by individual GABAergic interneurons. *Nature* **378**, 75–78 (1995).

15. Colgin, L. L. Rhythms of the hippocampal network. *Nat Rev Neurosci* **17**, 239–249 (2016).

16. Burgess, N. & O'Keefe, J. Models of place and grid cell firing and theta rhythmicity. *Current Opinion in Neurobiology* **21**, 734–744 (2011).

17. Niedermeyer, E. & Silva, F. H. L. da. *Electroencephalography: Basic Principles, Clinical Applications, and Related Fields*. (Lippincott Williams & Wilkins, 2005).

18. Quigley, C. Forgotten rhythms? Revisiting the first evidence for rhythms in cognition. *European Journal of Neuroscience* **55**, 3266–3276 (2022).

19. Contreras, D. & Steriade, M. Synchronization of low-frequency rhythms in corticothalamic networks. *Neuroscience* **76**, 11–24 (1996).

20. Steriade, M., McCormick, D. A. & Sejnowski, T. J. Thalamocortical Oscillations in the Sleeping and Aroused Brain. *Science* **262**, 679–685 (1993).

21. Jensen, O. & Mazaheri, A. Shaping Functional Architecture by Oscillatory Alpha Activity: Gating by Inhibition. *Front Hum Neurosci* **4**, 186 (2010).

22. Donoghue, J. P., Sanes, J. N., Hatsopoulos, N. G. & Gaál, G. Neural Discharge and Local Field Potential Oscillations in Primate Motor Cortex During Voluntary Movements. *Journal of Neurophysiology* **79**, 159–173 (1998).

23. Lebedev, M. A. & Wise, S. P. Oscillations in the premotor cortex: single-unit activity from awake, behaving monkeys. *Exp Brain Res* **130**, 195–215 (2000).

24. Baker, S. N., Olivier, E. & Lemon, R. N. Coherent oscillations in monkey motor cortex and hand muscle EMG show task-dependent modulation. *J Physiol* **501**, 225–241 (1997).

25. Feige, B., Aertsen, A. & Kristeva-Feige, R. Dynamic Synchronization Between Multiple Cortical Motor Areas and Muscle Activity in Phasic Voluntary Movements. *Journal of Neurophysiology* **84**, 2622–2629 (2000).

26. Mima, T., Matsuoka, T. & Hallett, M. Information flow from the sensorimotor cortex to muscle in humans. *Clinical Neurophysiology* **112**, 122–126 (2001).

27. Murthy, V. N. & Fetz, E. E. Oscillatory activity in sensorimotor cortex of awake monkeys: synchronization of local field potentials and relation to behavior. *J Neurophysiol* **76**, 3949–3967 (1996).

28. Murthy, V. N. & Fetz, E. E. Synchronization of neurons during local field potential oscillations in sensorimotor cortex of awake monkeys. *Journal of Neurophysiology* **76**, 3968–3982 (1996).

29. Bressler, S. L. Large-scale cortical networks and cognition. *Brain Research Reviews* **20**, 288–304 (1995).

30. Brovelli, A. *et al.* Beta oscillations in a large-scale sensorimotor cortical network: Directional influences revealed by Granger causality. *Proc Natl Acad Sci U S A* **101**, 9849–9854 (2004).

31. Nakamura, A., Miura, R., Suzuki, Y., Morasso, P. & Nomura, T. Discrete cortical control during quiet stance revealed by desynchronization and rebound of beta oscillations. 2023.05.01.539009 Preprint at https://doi.org/10.1101/2023.05.01.539009 (2023).

32. Buschman, T. J. & Miller, E. K. Top-Down Versus Bottom-Up Control of Attention in the Prefrontal and Posterior Parietal Cortices. *Science* **315**, 1860–1862 (2007).

33. Fries, P., Reynolds, J. H., Rorie, A. E. & Desimone, R. Modulation of Oscillatory Neuronal Synchronization by Selective Visual Attention. *Science* **291**, 1560–1563 (2001).

34. Bichot, N. P., Rossi, A. F. & Desimone, R. Parallel and Serial Neural Mechanisms for Visual Search in Macaque Area V4. *Science* **308**, 529–534 (2005).

35. Landfield, P. W., McGaugh, J. L. & Tusa, R. J. Theta Rhythm: A Temporal Correlate of Memory Storage Processes in the Rat. *Science* **175**, 87–89 (1972).

36. Tóth, K., Freund, T. F. & Miles, R. Disinhibition of rat hippocampal pyramidal cells by GABAergic afferents from the septum. *J Physiol* **500**, 463–474 (1997).

37. Hangya, B., Borhegyi, Z., Szilágyi, N., Freund, T. F. & Varga, V. GABAergic Neurons of the Medial Septum Lead the Hippocampal Network during Theta Activity. *J Neurosci* **29**, 8094–8102 (2009).

38. Goutagny, R., Jackson, J. & Williams, S. Self-generated theta oscillations in the hippocampus. *Nat Neurosci* **12**, 1491–1493 (2009).

39. Gupta, A. S., van der Meer, M. A. A., Touretzky, D. S. & Redish, A. D. Segmentation of spatial experience by hippocampal theta sequences. *Nat Neurosci* **15**, 1032–1039 (2012).

40. Wang, Y., Romani, S., Lustig, B., Leonardo, A. & Pastalkova, E. Theta sequences are essential for internally generated hippocampal firing fields. *Nat Neurosci* **18**, 282–288 (2015).

41. Lubenov, E. V. & Siapas, A. G. Hippocampal theta oscillations are travelling waves. *Nature* **459**, 534–539 (2009).

42. Yartsev, M. M., Witter, M. P. & Ulanovsky, N. Grid cells without theta oscillations in the entorhinal cortex of bats. *Nature* **479**, 103–107 (2011).

43. Yartsev, M. M. & Ulanovsky, N. Representation of Three-Dimensional Space in the Hippocampus of Flying Bats. *Science* **340**, 367–372 (2013).

44. Heys, J. G., MacLeod, K. M., Moss, C. F. & Hasselmo, M. E. Bat and Rat Neurons Differ in Theta-Frequency Resonance Despite Similar Coding of Space. *Science* **340**, 363–367 (2013).

45. Killian, N. J., Jutras, M. J. & Buffalo, E. A. A Map of Visual Space in the Primate Entorhinal Cortex. *Nature* **491**, 761–764 (2012).

46. Kahana, M. J., Sekuler, R., Caplan, J. B., Kirschen, M. & Madsen, J. R. Human theta oscillations exhibit task dependence during virtual maze navigation. *Nature* **399**, 781–784 (1999).

47. Colgin, L. L. Mechanisms and Functions of Theta Rhythms. *Annual Review of Neuroscience* **36**, 295–312 (2013).

48. Mitchell, J. F. & Leopold, D. A. The marmoset monkey as a model for visual neuroscience. *Neurosci Res* **93**, 20–46 (2015).

49. Cyranoski, D. Marmosets are stars of Japan's ambitious brain project. *Nature News* **514**, 151 (2014).

50. Walker, J., MacLean, J. & Hatsopoulos, N. G. The marmoset as a model system for studying voluntary motor control. *Devel Neurobio* **77**, 273–285 (2017).

51. Hunsaker, M. R., Scott, J. A., Bauman, M. D., Schumann, C. M. & Amaral, D. G. Postnatal Development of the Hippocampus in the Rhesus Macaque (Macaca mulatta): A Longitudinal Magnetic Resonance Imaging Study. *Hippocampus* **24**, 794–807 (2014).

52. Courellis, H. S. *et al.* Spatial encoding in primate hippocampus during free navigation. *PLoS Biol* **17**, e3000546 (2019).

53. Bukhtiyarova, O., Chauvette, S., Seigneur, J. & Timofeev, I. Brain states in freely behaving marmosets. *Sleep* **45**, zsac106 (2022).

54. Jutras, M. J., Fries, P. & Buffalo, E. A. Oscillatory activity in the monkey hippocampus during visual exploration and memory formation. *Proceedings of the National Academy of Sciences of the United States of America* **110**, 13144 (2013).

55. Johnston, K. D., Barker, K., Schaeffer, L., Schaeffer, D. J. & Everling, S. Methods for chair restraint and training of the common marmoset on oculomotor tasks. *Journal of Neurophysiology* (2018) doi:10.1152/jn.00866.2017.

56. Kim, H. Encoding and retrieval along the long axis of the hippocampus and their relationships with dorsal attention and default mode networks: The HERNET model. *Hippocampus* **25**, 500–510 (2015).

57. Fritch, H. A., Spets, D. S. & Slotnick, S. D. Functional connectivity with the anterior and posterior hippocampus during spatial memory. *Hippocampus* **31**, 658–668 (2021).

58. Piza, D. B. *et al.* The hippocampus of the common marmoset is a GPS, but G is for gaze. 2023.05.24.542209 Preprint at https://doi.org/10.1101/2023.05.24.542209 (2023).

59. Sheremet, A., Burke, S. N. & Maurer, A. P. Movement Enhances the Nonlinearity of Hippocampal Theta. *J Neurosci* **36**, 4218–4230 (2016).

60. Five Films. Stock photo of Common marmoset (Callithrix jacchus) running along a branch and jumping.... *Nature Picture Library* https://www.naturepl.com/stock-video-common-marmoset-callithrix-jacchus-running-along-a-branch-and-jumping-clip01530114.html (2016).

61. Donhauser, P. Spectral Analysis: How to process neural oscillatory signals. (2015).

62. Szymanski, L. J. *et al.* Neuropathological effects of chronically implanted, intracortical microelectrodes in a tetraplegic patient. *J. Neural Eng.* **18**, 0460b9 (2021).

63. Spyropoulos, G. *et al.* Spontaneous variability in gamma dynamics described by a damped harmonic oscillator driven by noise. *Nat Commun* **13**, 2019 (2022).

64. Fiebelkorn, I. C. & Kastner, S. A rhythmic theory of attention. *Trends Cogn Sci* **23**, 87–101 (2019).

65. Hayhoe, M. & Ballard, D. Eye movements in natural behavior. *Trends in Cognitive Sciences* **9**, 188–194 (2005).

66. McCrea, R. A. & Gdowski, G. T. Firing behaviour of squirrel monkey eye movement-related vestibular nucleus neurons during gaze saccades. *J Physiol* **546**, 207–224 (2003).

67. Burkart, J. & Heschl, A. Geometrical gaze following in common marmosets (Callithrix jacchus). *J Comp Psychol* **120**, 120–130 (2006).

68. Mitchell, J. F., Reynolds, J. H. & Miller, C. T. Active Vision in Marmosets: A Model System for Visual Neuroscience. *J Neurosci* **34**, 1183–1194 (2014).

69. Carriot, J., Jamali, M., Chacron, M. J. & Cullen, K. E. The statistics of the vestibular input experienced during natural self-motion differ between rodents and primates. *J Physiol* **595**, 2751–2766 (2017).

70. Ahmed, O. J. & Mehta, M. R. Running Speed Alters the Frequency of Hippocampal Gamma Oscillations. *J Neurosci* **32**, 7373–7383 (2012).

71. Aghajan, Z. M. *et al.* Theta Oscillations in the Human Medial Temporal Lobe during Real World Ambulatory Movement. *Curr Biol* **27**, 3743-3751.e3 (2017).

72. Mankin, E. A. *et al.* The hippocampal code for space in Mongolian gerbils. *Hippocampus* **29**, 787–801 (2019).

73. Noachtar, I., Harris, T.-A., Hidalgo-Lopez, E. & Pletzer, B. Sex and strategy effects on brain activation during a 3D-navigation task. *Commun Biol* **5**, 234 (2022).

74. Sneider, J. T. *et al.* Sex differences in spatial navigation and perception in human adolescents and emerging adults. *Behav Processes* **111**, 42–50 (2015).

# Appendices

| | |
|---|---|
| **PI :** | Martinez, Julio |
| **Protocol #** | 2020-137 |
| **Status :** | Approved (w/o Stipulation) |
| **Approved :** | 06/01/2021 |
| **Expires :** | 06/01/2025 |
| **Title :** | Role of Pre-Frontal Cortex and Amygdala in Cognitive Control in the Common Marmoset |

## Table of Contents



Protocol Introduction

The questions on this page activate specific sections within the AUP form.

Note that species selection is part of this introductory page

**Appendix A.** Copy of approved animal use protocol.

# Curriculum Vitae

| | |
|---|---|
| **Name:** | William JM Assis |
| **Post-secondary Education and Degrees:** | Western University<br>London Ontario, Canada<br>2012-2016 BMSc |
| **Related Work Experience** | Teaching Assistant<br>Western University<br>2019-2023 |
| | Research Assistant<br>Western University<br>2014-2016 |